

See discussions, stats, and author profiles for this publication at: <https://www.researchgate.net/publication/277599301>

Probing the Hydrogen Bonding of the Ferrous–NO Heme Center of nNOS by Pulsed Electron Paramagnetic Resonance

ARTICLE in THE JOURNAL OF PHYSICAL CHEMISTRY A · JUNE 2015

Impact Factor: 2.69 · DOI: 10.1021/acs.jpca.5b01804 · Source: PubMed

READS

30

9 AUTHORS, INCLUDING:



Bradley Elmore

University of New Mexico

25 PUBLICATIONS 346 CITATIONS

SEE PROFILE



Huiying Li

University of California, Irvine

106 PUBLICATIONS 3,670 CITATIONS

SEE PROFILE



Thomas L Poulos

University of California, Irvine

164 PUBLICATIONS 4,538 CITATIONS

SEE PROFILE



Changjian Feng

University of New Mexico

60 PUBLICATIONS 1,038 CITATIONS

SEE PROFILE

1 Probing the Hydrogen Bonding of the Ferrous–NO Heme Center of 2 nNOS by Pulsed Electron Paramagnetic Resonance

3 Andrei V. Astashkin,[†] Li Chen,[‡] Bradley O. Elmore,[‡] Deepak Kunwar,[‡] Yubin Miao,[‡] Huiying Li,[§]
4 Thomas L. Poulos,[§] Linda J. Roman,^{||} and Changjian Feng^{*,‡}

5 [†]Department of Chemistry and Biochemistry, University of Arizona, Tucson, Arizona 85721, United States

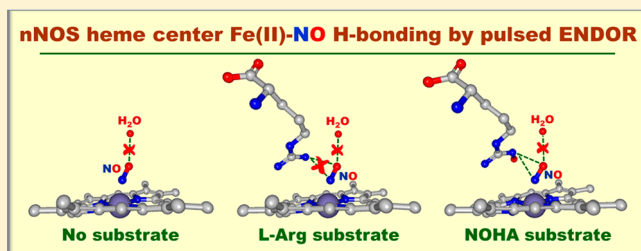
6 [‡]College of Pharmacy, University of New Mexico, Albuquerque, New Mexico 87131, United States

7 [§]Departments of Molecular Biology and Biochemistry, Chemistry, and Pharmaceutical Sciences, University of California, Irvine,
8 Irvine, California 92697-3900, United States

9 ^{||}Department of Biochemistry, University of Texas Health Science Center in San Antonio, San Antonio, Texas 78229, United States

10 **S** Supporting Information

11 **ABSTRACT:** Oxidation of L-arginine (L-Arg) to nitric oxide
12 (NO) by NO synthase (NOS) takes place at the heme active
13 site. It is of current interest to study structures of the heme
14 species that activates O₂ and transforms the substrate. The
15 NOS ferrous–NO complex is a close mimic of the obligatory
16 ferric (hydro)peroxo intermediate in NOS catalysis. In this
17 work, pulsed electron–nuclear double resonance (ENDOR)
18 spectroscopy was used to probe the hydrogen bonding of the
19 NO ligand in the ferrous–NO heme center of neuronal NOS
20 (nNOS) without a substrate and with L-Arg or N-hydroxy-L-
21 arginine (NOHA) substrates. Unexpectedly, no H-bonding interaction connecting the NO ligand to the active site water
22 molecule or the Arg substrate was detected, in contrast to the results obtained by X-ray crystallography for the Arg-bound nNOS
23 heme domain [Li et al. *J. Biol. Inorg. Chem.* **2006**, *11*, 753–768]. The nearby exchangeable proton in both the no-substrate and
24 Arg-containing nNOS samples is located outside the H-bonding range and, on the basis of the obtained structural constraints,
25 can belong to the active site water (or OH). On the contrary, in the NOHA-bound sample, the nearby exchangeable hydrogen
26 forms an H-bond with the NO ligand (on the basis of its distance from the NO ligand and a nonzero isotropic *hfi* constant), but
27 it does not belong to the active site water molecule because the water oxygen atom (detected by ¹⁷O ENDOR) is too far. This
28 hydrogen should therefore come from the NOHA substrate, which is in agreement with the X-ray crystallography work [Li et al.
29 *Biochemistry* **2009**, *48*, 10246–10254]. The nearby nonexchangeable hydrogen atom assigned as H_e of Phe584 was detected in all
30 three samples. This hydrogen atom may have a stabilizing effect on the NO ligand and probably determines its position.



31 INTRODUCTION

32 Mammalian nitric oxide synthases (NOSs) are enzymes
33 responsible for oxidation of L-arginine (L-Arg) to nitric oxide
34 (NO).¹ These reactions occur at the heme active site(s) in the
35 oxygenase domain of NOS. Their mechanistic aspects are not
36 completely understood,² and it is of current interest to study
37 structures of the heme species that activates O₂ and transforms
38 the substrate.³ Knowledge of the relative structural arrangement
39 of the heme, substrate, and possible other molecules relevant to
40 catalysis is important for understanding the chemical
41 mechanism. One specific, important problem is the role of
42 hydrogen bonding, and in this context, of the active site water
43 molecule, in the catalysis. According to the X-ray structures, a
44 single water molecule is within H-bonding distance from the
45 diatomic ligand (O₂) and is proposed to provide at least one of
46 the protons necessary for promoting heterolytic cleavage of the
47 O–O bond followed by oxidation of L-Arg to N-hydroxy-L-
48 arginine (NOHA) and then to NO.⁴

Electron paramagnetic resonance (EPR) is a powerful tool
for elucidating protein/enzyme structures both at the level of
local environment of the enzyme active site(s)⁵ and at the level
of the overall protein geometry and folding (using site-directed
spin labeling).⁶ In addition to complementing X-ray crystallog-
raphy by providing structural information in solution, EPR also
can directly detect the presence of protons in the vicinity of a
paramagnetic center. Importantly, it can determine if a
hydrogen bond is formed between a particular hydrogen and
the paramagnetic center.⁷

One of the most crucial and interesting paramagnetic
intermediates in the catalytic NOS heme domain, the ferric
(hydro)peroxo heme complex, is extremely reactive⁸ and
presents serious challenges for direct EPR detection. However,
various indirect approaches to EPR investigations of the heme

Received: February 23, 2015

Revised: May 7, 2015

active site structure in this state can be employed. In some of the works by Brian Hoffman's group,^{7b,9} the ferric intermediate was generated by using a cryoreduction technique. As a more accessible alternative, we have recently started pulsed EPR study of a stable ferrous nitrosyl form of NOS heme centers, which is isoelectronic to the native ferric (hydro)peroxo intermediate in NOS.¹⁰ Another advantage of this approach is that a significant spin density is localized on the NO ligand, which improves EPR sensitivity to the structural details of the second coordination sphere.

Using this approach, we have previously obtained information on the position of the L-Arg substrate relative to the NO ligand of the ferrous–NO heme center of neuronal NOS (nNOS) and compared it with the crystal structure.¹¹ It was found that the L-Arg position in frozen solution is noticeably different from that in the crystal, with the shifts of some of the atoms as large as 1 Å. This result shows that although the crystal structures provide valuable guidance regarding the relative position of various structural elements of the protein and the substrate, a certain amount of caution should be exercised when these structures are used for making conclusions about possible interactions between the molecular components in solution. This is particularly significant in the case of the hydrogen bonding because a ~ 1 Å shift in the relative position of the potential hydrogen bonding partners may correspond to two qualitatively different chemical situations of the H-bond being either present or absent. In the present work, we used the pulsed electron–nuclear double resonance (ENDOR) at the microwave (mw) K_2 band (~ 30 GHz) to probe the hydrogen bonding of the NO ligand in the ferrous–NO nNOS samples without a substrate and with the L-Arg or NOHA substrate.

MATERIALS AND METHODS

1. EPR Sample Preparation. Rat nNOS oxygenase (NOSoxy) construct, in which only the heme-containing oxygenase domain is present, was expressed and purified as reported earlier.¹² Three types of EPR samples were prepared in the H_2O , D_2O , or $H_2^{17}O$ buffers: without substrate, with L-Arg, or with NOHA. Buffer exchange into D_2O was accomplished by concentrating the protein samples to 20 μL and then diluting to 0.5 mL with the appropriate buffer in D_2O . This procedure was repeated three times. The value of pD was calculated as described by Glasoe and Long,¹³ i.e., $pD_{\text{true}} = pD_{\text{apparent}} + 0.4$. The ^{17}O -enrichment was accomplished by mixing the protein sample with 70% $H_2^{17}O$ buffer (final $H_2^{17}O$ concentration: $\sim 50\%$). The EPR samples were then prepared in a septum-sealed quartz cuvette (Starna Cells, 9/Q/10-GL14-S). A 300 μL aliquot of 500 μM nNOSoxy was added into the cuvette; buffer: 100 mM Bis–Tris–propane, 200 mM NaCl, 1 mM DTT, 10 μM H_4B , 10% glycerol, pH 7.4. The protein solution was deoxygenated with three cycles of vacuum pumping and purging (with dioxygen-scrubbed argon gas). NO gas was introduced into the headspace until complete disappearance of the high spin ferric heme band at 650 nm, indicative of the formation of the ferric–NO adduct. The sample was then reduced with excess amount of freshly prepared dithionite solution. To prepare the substrate-containing samples, solid L-Arg hydrochloride or NOHA monoacetate salt was added to a final concentration of 10 mM; the change in pH of the sample was negligible. A ~ 45 μL sample was then transferred into an EPR tube and rapidly frozen in a pentane and liquid nitrogen slurry.

2. Pulsed EPR Experiments. The pulsed EPR experiments were performed on a home-built broadband (26–40 GHz) K_2 -band pulsed EPR spectrometer.¹⁴ The specific techniques used in this work to detect the ^{17}O and $^1H/^2H$ ENDOR spectra were the regular Mims ENDOR¹⁵ and the refocused Mims ENDOR techniques,^{7a,16} respectively. The detailed experimental conditions are given in the figure captions. The numerical simulations of the ENDOR spectra were performed using the SimBud software.¹⁷

RESULTS AND DISCUSSION

1. Structural Background. In this work, we investigated the H-bonding of the NO ligand of the ferrous heme center of nNOS in the preparations without substrates and with L-Arg or NOHA substrate. For simplicity of reference, these respective samples are denoted nNOS/NS (“NS” stands for “No Substrate”), nNOS/Arg, and nNOS/NOHA. The relevant X-ray structures available in the protein data bank and described in the literature are those of the ferrous–NO form of the oxygenase domain of nNOS/Arg (pdb 2G6K) and nNOS/NOHA (pdb 3HSP). Figure 1 shows the relative positions of

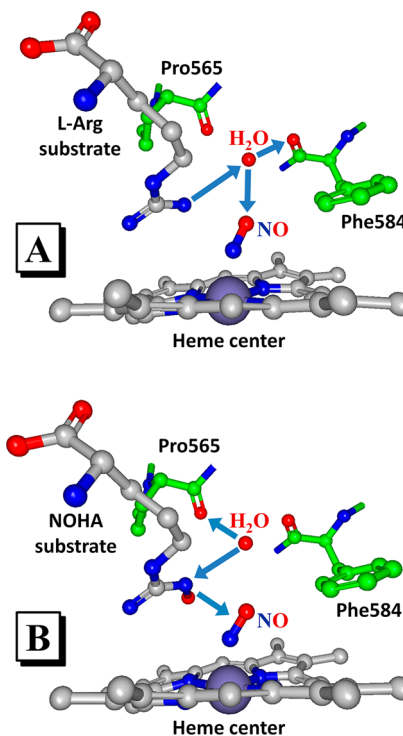


Figure 1. Structures of heme active sites of nNOS/Arg (panel A, pdb 2G6K) and nNOS/NOHA (panel B, pdb 3HSP). The arrows show the potential H-bonds between the active site water, substrate, the NO ligand and nearby residues, as identified on the basis of the distance and angle considerations in the X-ray investigations⁴ (the arrow direction is from the H-bond donor to the acceptor).

the NO-coordinated heme, the substrate, the oxygen of the active site water molecule, and the nearby amino acid residues implicated in the H-bonding with the active site water. The arrows in Figure 1 show the potential H-bonds between the active site water, substrate, and the NO ligand, as identified on the basis of the local geometric considerations in the X-ray investigations.⁴ To the best of our knowledge, no X-ray structures for the ferrous–NO form of the oxygenase domain of nNOS/NS are available.

Table 1. Distances to N_{NO} and O_{NO}, and Estimated Anisotropic *hfi* Constants for the Nearest Non-Exchangeable Proton (H_e of F584) and the Oxygen Atom of the Active Site Water Molecule in the nNOS Subunits A and B^a

atom	dist to N _{NO} (Å)	dist to O _{NO} (Å)	<i>T</i> (MHz) for $\rho(\text{Fe,N,O}) = (0.2, 0.5, 0.3)$	<i>T</i> (MHz) for $\rho(\text{Fe,N,O}) = (0.2, 0.7, 0.1)$	exptl <i>T</i> (MHz)
¹ H _e of F584 in nNOS/NS					7.65
¹ H _e of F584 in nNOS/Arg	3.24 (3.03)	2.41 (2.22)	5.77 (7.19)	4.55 (5.54)	7.65
¹ H _e of F584 in nNOS/NOHA	3.21 (3.25)	2.43 (2.36)	5.90 (5.94)	4.67 (4.58)	7.65
¹⁷ O _{H₂O} in nNOS/NS					−0.36
¹⁷ O _{H₂O} in nNOS/Arg	3.76 (4.08)	2.95 (2.99)	−0.46 (−0.42)	−0.38 (−0.32)	−0.27
¹⁷ O _{H₂O} in nNOS/NOHA	3.92 (4.04)	3.04 (3.16)	−0.42 (−0.38)	−0.35 (−0.31)	−0.23
¹⁵ N _{g1} in nNOS/Arg	2.97 (3.07)	3.06 (2.87)	−0.48 (−0.48)	−0.50 (−0.48)	−0.93
¹ H _{exch} in nNOS/NS					3.1
¹ H _{exch} in nNOS/Arg	2.8 (3.08)	1.95 (1.99)	9.88 (8.90)	7.28 (6.00)	2.8
¹ H _{exch} in nNOS/NOHA	2.58 (2.86)	2.10 (2.47)	8.96 (6.39)	7.99 (5.89)	5.7
¹ H _δ of L-Arg in nNOS/Arg	3.06 (2.98)	2.41 (2.57)	6.11 (5.71)	5.13 (5.23)	2.35

^aThe structural parameters are obtained from pdb 2G6K and 3HSP. The distances and calculated *T*_{||} values without and within parentheses correspond to subunits A and B, respectively. The experimental *T*_{||} values for the L-Arg ¹H_δ and ¹⁵N_{g1} are from ref 16.

2. Approach and Complications. To detect the H-bonding of the NO ligand, ¹H, ²H, and ¹⁷O ENDOR experiments were performed with the samples prepared in H₂O, D₂O, and H₂¹⁷O. The ²H ENDOR and the “H₂O – D₂O” difference ¹H ENDOR spectra show the deuterons and the exchangeable protons, respectively. The distances from the NO ligand to the exchangeable protons are estimated from the anisotropic *hfi* that is found from the analysis of the ENDOR spectra. These distances represent the basis for making a decision regarding possible H-bonding. To qualify as H-bonds, these distances should be smaller than the sum of the van der Waals radii of N or O, ~1.55 and 1.52 Å, respectively, and H, ~1.2 Å. In addition, a nonzero isotropic *hfi* constant is expected in the case of an H-bond. The ¹⁷O spectra mostly play an auxiliary role: they help to establish if the H-bonded hydrogen(s) could belong to the nearby active site water.

To estimate the distance from the NO ligand to a particular proton (or another magnetic nucleus) from its *hfi* anisotropy, one must take into account the distribution of the electronic spin density over the Fe–NO fragment. Several distributions were estimated by density functional theory (DFT) calculations^{7c,d,18} ranging from ($\rho_{\text{Fe}}, \rho_{\text{NO}}$) ≈ (0.74, 0.26) to (−0.2, +1.2). The analysis of the ENDOR spectra from L-Arg substrate enriched in ²H at carbon positions and ¹⁵N at guanidino nitrogens in our previous work¹¹ has shown that the intermediate spin population distribution with ($\rho_{\text{Fe}}, \rho_{\text{NO}}$) ≈ (0.2, 0.8) predicted in some of the DFT studies^{18b,c,19} is the most realistic one, and we will continue using such a distribution in this work. The relative spin populations on N and O were found to be about 1:0.6,²⁰ which results in the absolute spin populations of $\rho_{\text{N}} = 0.5$ and $\rho_{\text{O}} = 0.3$.

The second complication arises from the fact that at least in some of the X-ray structures of NOS oxygenase domain the orientations of the NO ligand for the two heme sites, A and B, are noticeably different (Figure S1, Supporting Information).^{4b} This could present problems with interpreting the EPR data if NO orientational heterogeneity also is present in frozen solution. In our previous work,¹¹ we have shown that in the case of such orientation differences, the magnitudes of the anisotropic *hfi* tensor components are affected significantly less (in fact, they are nearly invariant at sufficiently large distances) than the orientations of the *hfi* tensors with respect to the *g*-frame, which is linked to the NO-ligand orientation. This

conclusion is also supported by the anisotropic *hfi* values calculated for the relevant magnetic nuclei using the crystal structures (Table 1). The possible orientational inhomogeneity of the *hfi* tensors makes the analysis of the orientation-selective ENDOR spectra extremely difficult, especially taking into account the fact that they are contributed to by multiple nuclei. To simplify the data interpretation, similar to our previous work,¹¹ we used in our analysis the field-integrated (FI) ENDOR spectra²¹ obtained as weighted sums of the normalized (by the ESE amplitude without RF) orientation-selective spectra aligned at the Zeeman frequency of the nucleus of interest (in this work, ¹H or ¹⁷O), with the statistical weights given by the relative amplitudes of the ESE signal at the corresponding measurement positions (i.e., $p_k = A_k / \sum_j A_j$, where p_k is the statistical weight of the *k*th orientation-selective ENDOR spectrum and A_i are the field-sweep ESE spectrum amplitudes at the ENDOR measurement positions). The FI spectra represent an approximation to the spectra that would be obtained in the orientationally nonselective situation (in this case, for the hypothetical situation of isotropic *g*-factor of Fe(II)–NO center).

3. Field Sweep Spectra. Figure 2 shows the electron spin echo (ESE) field sweep spectra obtained at the mw K_a band (~30 GHz) for the samples of nNOS/NS, nNOS/Arg, and nNOS/NOHA (numerical first derivatives of these spectra are shown in Figure S2 of the Supporting Information). One can see that the spectra of nNOS/NS and nNOS/Arg are nearly identical and exhibit a resolved triplet structure at the intermediate turning point, *g_y*, due to the *hfi* of the ¹⁴N nucleus that belongs to the NO ligand (*A_y* ≈ 2.1 mT). The spectrum of nNOS/NOHA is very different, with smaller overall *g*-anisotropy, but significantly greater *g*-strain broadening, which obliterates the hyperfine structure at *g_y*.

The principal *g*-values determined from these spectra are (*g_x*, *g_y*, *g_z*) ≈ (1.969, 2.003, 2.083) for nNOS/NS, (*g_x*, *g_y*, *g_z*) ≈ (1.969, 2.003, 2.084) for nNOS/Arg, and (*g_x*, *g_y*, *g_z*) ≈ (1.985, 2.007, 2.076) for nNOS/NOHA. These principal *g*-values are mostly in good agreement with those determined by continuous wave EPR at the X-band.^{10b} The only notable difference is the intermediate *g*-value of nNOS/NOHA, 2.007 in this work vs 2.021 estimated at X-band. The value found in this work is more accurate because the assignment of the EPR turning points at K_a-band is straightforward due to a higher

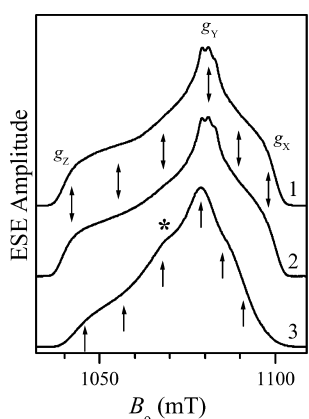


Figure 2. Two-pulse ESE field sweeps of ferrous-NO heme centers in nNOS/NS (trace 1), nNOS/Arg (trace 2), and nNOS/NOHA (trace 3). The arrows indicate the EPR positions, at which the ENDOR spectra were measured. The B_0 values (in mT) corresponding to the indicated EPR positions: (1042, 1055, 1068, 1081, 1089.5, 1098) for nNOS/NS and nNOS/Arg and (1045.8, 1056.8, 1067.8, 1078.8, 1084.8, 1090.8) for nNOS/NOHA. Experimental conditions: mw frequency, 30.305 GHz; mw pulses, 15 and 22 ns; time interval between the mw pulses, $\tau = 200$ ns; temperature, 15 K. The asterisk indicates a commonly observed minor feature of unknown origin (see Figures S2 and S3 in the Supporting Information for a numerical simulation).

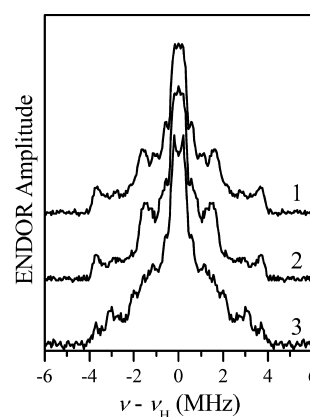


Figure 3. Refocused Mims ENDOR spectra of nonexchangeable protons in the vicinity of ferrous-NO heme centers of nNOS/NS, nNOS/Arg, and nNOS/NOHA in D_2O (traces 1–3, respectively) at the EPR position where the largest ENDOR splitting is observed ($B_0 = 1068$ mT for nNOS/NS and nNOS/Arg; $B_0 = 1067.8$ mT for nNOS/NOHA). Experimental conditions: mw frequency, 30.305 GHz; mw pulses, 15, 15, 15, and 22 ns; time interval between the first and second pulses, $\tau = 80$ ns; time interval between the second and third pulses, $T = 20$ μ s; time interval between the third and fourth pulses, $t = 280$ ns; RF pulse length, 18 μ s; temperature, 15 K.

magnetic field, B_0 , of $\theta_B \approx 52^\circ \pm 6^\circ$ (depending on the azimuthal angle of B_0 in the g -frame).

To obtain structural information for a magnetic nucleus (proton or ^{17}O) from its anisotropic hfi , the following approach was used. The possible positions of the nucleus with respect to the NO ligand were calculated using the three-point spin density distribution ($\rho_{Fe}, \rho_N, \rho_O$) = (0.2, 0.5, 0.3) described above. Specifically, the anisotropic hfi tensor was calculated for a trial position of the magnetic nucleus, and this position was varied until the agreement with the experimental $T_{||}$ value was reached. For any given $T_{||}$ value, the solution is not unique, and the whole set of solutions represents a surface enveloping the Fe-NO fragment.

Because ρ_{Fe} is small, the solution surface has a near-cylindrical symmetry with respect to the N-O bond in the part of space distant from the Fe(II) ion (i.e., where the studied second sphere nuclei are located). For this part of space, the obtained possible positions for a given magnetic nucleus can be presented by a line in the XY coordinate system with axis X coinciding with the N-O bond and the nitrogen atom located at the coordinate origin. This line represents an intersection of the solution surface with the XY plane. The direction of axis Y is generally different for each magnetic nucleus: it is selected in such a way that this nucleus is located in the (++) quadrant of the XY plane. As a consequence of the near-cylindrical symmetry, the 2D position estimates virtually do not depend on the specific orientation of axis Y as long as it points in a general direction parallel to or away from the heme plane and the heme Fe atom. Such a flexible definition of the Y axis allows one to conveniently present the positions of all relevant surrounding magnetic nuclei on the XY plane. The above description of the XY coordinate system implies that the Fe(II) ion, which is not explicitly shown in the plots, is located at $X_{Fe} \approx -1.53$ Å and $Y_{Fe} \in [-0.92, 0]$ Å, depending on specific orientation of the Y-axis. Such XY coordinate system is used in Figures 4 and 6 below.

The calculated range of possible positions of the non-exchangeable proton with $T_{||} = 7.65$ MHz is shown by the solid

Zeeman resolution, whereas at the X-band the g_y region of the spectrum is complicated, making a definitive assignment difficult.^{10b}

The feature marked by an asterisk is located at $g \approx 2.027$. It is the largest in the spectrum of nNOS/NOHA, but in the other two spectra it is also present, although with a smaller amplitude. This feature was observed in ferrous-NO samples of various heme proteins,^{7c,d,22} and its origin is not entirely clear. The DFT calculations suggest that it could result from a 5-coordinate heme with the NO ligand in an eclipsed conformation, i.e., when the Fe-NO plane (approximately) coincides with the $N_{(NO)}-Fe-N_{(porph)}$ plane.^{18a} This would indicate that in a minor fraction of the nNOS heme sites the cysteine ligand could have (partially) dissociated. A numerical simulation (Figures S2 and S3, Supporting Information) shows that the contribution of this species to the ESE signal for nNOS/NOHA sample does not exceed 15%. Therefore, regardless of the origin, such a minor species does not interfere with the analysis of the ENDOR data, where only major ENDOR lines are considered.

4. ENDOR Spectra of Nonexchangeable Protons.

Figure 3 shows the ENDOR spectra of nonexchangeable protons obtained at the EPR positions where the largest splitting between the ENDOR lines is observed (see Figure S4 of Supporting Information for the full set of the orientation-selective spectra). The largest splitting is achieved at the EPR position approximately 13 mT (for nNOS/NS and nNOS/Arg) or 11 mT (nNOS/NOHA) downfield from g_y , and it equals to about 7.65 MHz. Assuming the isotropic hfi constant, a_{iso} , to be zero, which is reasonable for nonexchangeable protons, one can equate this splitting with the largest component of the anisotropic hfi tensor, $T_{||}$ (in spite of a possibility of some nonaxiality of the hfi tensor, we will still retain the notation $T_{||}$ for this component). This EPR position corresponds to the angle between the axis of g_z and the vector of the external

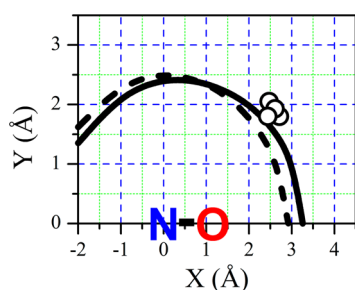


Figure 4. Position of H_e of Phe584 with respect to the NO ligand. Black lines show the range of possible positions predicted on the basis of $T_{\parallel} = 7.65$ MHz using the spin density distributions $(\rho_{Fe}, \rho_{N}, \rho_O) = (0.2, 0.5, 0.3)$ (solid line) and $(\rho_{Fe}, \rho_{N}, \rho_O) = (0.2, 0.7, 0.1)$ (dashed line). Open circles are the positions of Phe584 H_e in nNOS/Arg and nNOS/NOHA predicted from crystal structures (pdb 2G6K and 3HSP, respectively).

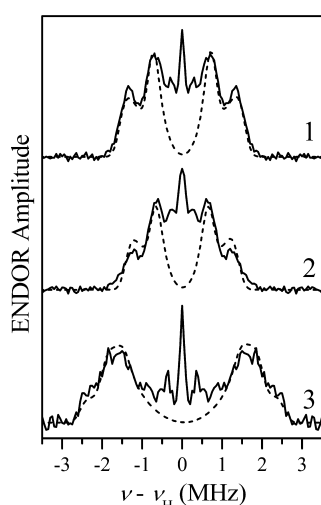


Figure 5. Field-integrated refocused Mims ENDOR of exchangeable protons in the vicinity of ferrous–NO heme centers of nNOS/NS, nNOS/Arg, and nNOS/NOHA (traces 1–3, respectively). Solid traces are experimental results, obtained as differences between the ENDOR spectra of samples in H_2O and D_2O (the original orientation-selective spectra used to calculate the FI spectra are shown in Figure S4 of Supporting Information). Experimental conditions are the same as in Figure 3. Dashed traces are simulations with $(a_{iso}, T_{11}, T_{22}, T_{33}) = (0, -1.55, -1.55, +3.1)$ MHz for nNOS/NS, $(0, -1.4, -1.4, +2.8)$ MHz for nNOS/Arg, and $(-0.6, -3.4, -2.3, +5.7)$ MHz for nNOS/NOHA. In the above notation, T_{33} corresponds to T_{\parallel} used for simplicity in the text. The accuracy of T_{33} is ± 0.1 MHz, and the corresponding accuracy for T_{11} and T_{22} is ± 0.05 MHz. The formal accuracy for a_{iso} is ± 0.05 MHz, but because the exchangeable protons for nNOS/NS and nNOS/Arg are beyond the H-bonding range (Figure 6), a_{iso} in these samples is strictly zero for all practical purposes. Individual Gaussian line widths were 0.25 MHz in all simulations.

black line in Figure 4. The analysis of the X-ray structures shows that the closest proton to the NO ligand is H_e of Phe 584 (Figure S1 of the Supporting Information). The positions of this proton obtained from several X-ray structures are shown by black open circles. Good agreement between the X-ray and ENDOR distances in this case provides extra support to the spin density distribution $(\rho_{Fe}, \rho_{N}, \rho_O) = (0.2, 0.5, 0.3)$ used in our distance calculations.

The angles θ_B calculated for H_e of Phe 584 using the X-ray structures of nNOS/Arg and nNOS/NOHA are within the range of 50 – 56° , in agreement with the experimental ENDOR

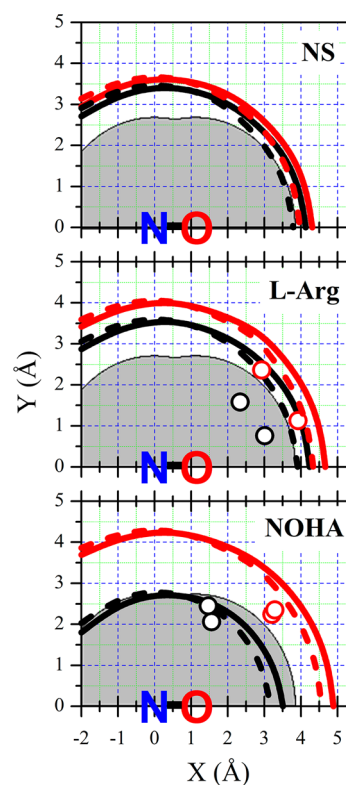


Figure 6. Positions of the nearby exchangeable proton (black) and active site water oxygen (red) with respect to the NO ligand. Solid and dashed lines (calculated using $(\rho_{Fe}, \rho_{N}, \rho_O) = (0.2, 0.5, 0.3)$ and $(0.2, 0.7, 0.1)$, respectively) show the possible positions predicted on the basis of the experimental T_{\parallel} values. Open circles show the proton and oxygen positions predicted or directly read from crystal structures (pdb 2G6K and 3HSP).

observations. In these estimates, the g -tensor orientation established both by DFT calculations and by X-ray crystallography for the 6-coordinated ferrous–NO heme centers⁴ was used, with the axis of g_z lying in the heme plane, perpendicular to the Fe–NO plane, and the axis of g_x approximately coinciding with the direction of the NO bond.

5. ENDOR Spectra of Exchangeable Protons. Figure 5 shows the FI 1H ENDOR spectra obtained as a difference between those recorded for the samples prepared in H_2O and D_2O (the original orientation-selective spectra used to calculate the FI spectra are shown in Figure S4 of the Supporting Information). The difference spectra of nNOS/NS and nNOS/Arg are significantly narrower than that of nNOS/NOHA. The numerical simulations of the spectra (dashed lines in Figure 5) show that while in the first two cases the hfi is purely anisotropic ($a_{iso} = 0$), in the last case a noticeable isotropic hfi constant is present ($a_{iso} \approx -0.6$ MHz). The anisotropic hfi in the cases of nNOS/NS and nNOS/Arg is with good accuracy axial, with T_{\parallel} about 3 MHz. In the case of nNOS/NOHA, the anisotropic hfi is noticeably rhombic and is about twice as strong: $T_{\parallel} \approx 5.7$ MHz.

The solid black lines in Figure 6 show the possible positions of the nearby exchangeable protons with respect to the NO ligand calculated on the basis of the T_{\parallel} values obtained from ENDOR and using $(\rho_{Fe}, \rho_{N}, \rho_O) = (0.2, 0.5, 0.3)$. The shaded area indicates the H-bonding distance range defined as the sum of the van der Waals radii of H and N or O. One can see that for the nNOS/NS and nNOS/Arg samples the nearby

exchangeable proton is outside the H-bonding range, whereas in the case of NOHA it is within the H-bonding range. A weak H-bond with NOHA is consistent with the nonzero isotropic hfi constant ($a_{iso} \approx -0.6$ MHz; see above). The assignment of the H-bonding hydrogen in the nNOS/NOHA sample is discussed below.

6. ^{17}O ENDOR Spectra. Figure 7 shows the ^{17}O FI ENDOR spectra obtained for samples prepared with ^{17}O -

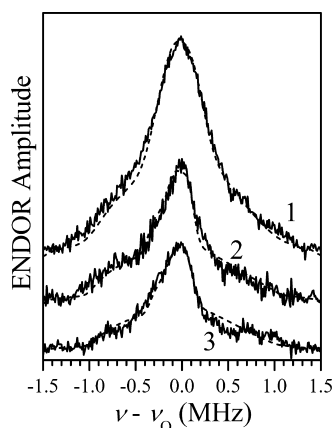


Figure 7. Field-integrated Mims ENDOR spectra of exchangeable ^{17}O in the vicinity of ferrous-NO heme centers of nNOS/NS, nNOS/Arg, and nNOS/NOHA in H_2^{17}O (traces 1–3, respectively). Solid traces are experimental results (the original orientation-selective spectra used to calculate the FI spectra are shown in Figure S5 of Supporting Information). Experimental conditions: mw frequency, 30.305 GHz; mw pulses, 15, 15, and 15 ns; time interval between the first and second pulses, $\tau = 700$ ns; time interval between the second and third pulses, $T = 15$ μs ; RF pulse length, 10 μs ; temperature, 15 K. Dashed traces are simulations with $a_{iso} = 0$ (for all traces) and $T_{||} = -0.36$ MHz for nNOS/NS, -0.27 MHz for nNOS/Arg, and -0.23 MHz for nNOS/NOHA. The nqi parameters were $e^2Qq/h = 6.5$ MHz and $\eta = 1$. The orientation of the nqi frame with respect to the hfi one is described by the Euler angles $(\theta_{hq}, \psi_{hq}) = (60^\circ, 30^\circ)$, $(40^\circ, 50^\circ)$, and $(40^\circ, 50^\circ)$ for nNOS/NS, nNOS/Arg, and nNOS/NOHA, respectively (the angle ϕ_{hq} is arbitrary because the hfi tensor is axial. See the Supporting Information for the Euler angles definition). Individual Gaussian line widths were 0.2 MHz for nNOS/NS and 0.1 MHz for nNOS/Arg and nNOS/NOHA. See the Supporting Information for the simulation details. Simulation examples using other parameters are also presented in Figures S6 and S7 of the Supporting Information.

enriched water (solid lines; the original orientation-selective spectra used to calculate the FI spectra are shown in Figure S5 of the Supporting Information). These spectra exhibit two distinct features: the relatively narrow central peak due to the $+1/2 \leftrightarrow -1/2$ transition of ^{17}O (the noticeable asymmetry of this peak is caused by the second order effects of the nqi) and a broad background peak mostly contributed to by $\pm 1/2 \leftrightarrow \pm 3/2$ transitions. The lines of $\pm 3/2 \leftrightarrow \pm 5/2$ transitions are about twice as broad and about one-half in amplitude. Our approach to the numerical simulations of these spectra is described in the Supporting Information. The results of the simulations are shown by the dashed lines in Figure 7. In contrast to the exchangeable protons results (see the anisotropic hfi values above), the weakest ^{17}O hfi is observed for nNOS/NOHA ($T_{||} = -0.23 \pm 0.02$ MHz), whereas the strongest one is found for the nNOS/NS sample ($T_{||} = -0.36 \pm 0.05$ MHz).

The red lines in Figure 6 show the possible positions of the active site water oxygen for each of the samples obtained from

the analysis of the ^{17}O anisotropic hfi . One can see that for the nNOS/NS and nNOS/Arg samples the minimal projection of the distance between the nearby exchangeable proton and the ^{17}O on the XY plane of the figure is shorter than the OH bond length of ~ 1 Å. This indicates that the nearby exchangeable proton detected by ENDOR can belong to the active site water molecule. In contrast, the projection of the H–O distance on the XY plane in the case of nNOS/NOHA is at least 1.4 Å, significantly greater than the OH bond length. It thus follows that the nearby exchangeable proton in nNOS/NOHA cannot belong to the active site water molecule. The most likely other H-bonding candidate in this case is the NH hydrogen of NOHA, as suggested in the X-ray crystallographic work.^{4a}

7. Comparison with the Crystal Structures. The red open circles in Figure 6 indicate the positions of the active site water oxygen atom in the crystal structures of nNOS/Arg and nNOS/NOHA (for nNOS/NS no X-ray data are available). The ~ 3 Å distance between this oxygen atom and the NO ligand observed in the crystal structures was interpreted as pointing at the existence of a hydrogen bond between these two moieties, at least in nNOS/Arg (for nNOS/NOHA, the water molecule was suggested to be an H-bond donor to the nitrogen of the NH–OH group of NOHA; see Figure 1B).^{4b} The positions of the water hydrogen in the nNOS/Arg active sites predicted from the crystallographic positions of the water oxygen in the heme sites A and B are shown by black open circles in the middle panel of Figure 6.

Although the water oxygen positions estimated by ENDOR are at least 0.5 Å longer than those obtained by X-ray crystallography, they formally allow a similar interpretation in terms of potential H-bonding with the NO ligand. For instance, using the ^{17}O position obtained by ENDOR for nNOS/Arg, one could place the water hydrogen marginally within the H-bonding distance range: at least for the $\text{O}_{\text{NO}}-\text{N}_{\text{NO}}-\text{O}_{\text{water}}$ angles under 30° , the $\text{O}_{\text{NO}}-\text{H}$ distance predicted from the ^{17}O position would be ~ 2.5 – 2.6 Å. The latter distance could even be shortened to ~ 2.4 Å by considering a stronger ^{17}O anisotropic hfi at the margin of the error limits (-0.3 Å rather than the median value of -0.27 Å). Fortunately, however, with the magnetic resonance approach one does not need to make such predictions because the protons (unlike in the X-ray crystallography) are observable directly and the distances to them are readily obtained from the analysis of the ^1H ENDOR data. This direct estimate (solid black line in Figure 6) places the nearby exchangeable proton in nNOS/Arg outside the H-bonding range.

Thus, although both the X-ray and ENDOR water oxygen positions in nNOS/Arg are formally within the H-bonding range from the NO ligand, the ^1H ENDOR data for the frozen solution sample show definitively that the exchangeable protons are outside the H-bonding range. It is not clear, however, if the latter observation reflects an actual difference with the situation in a crystal sample studied by the X-ray crystallography because the hydrogen atoms are not directly observed by the X-ray, and it may be difficult to unequivocally assign the actual H-bond partner(s) on the basis only on the positions of heavier atoms such as oxygen.

For nNOS/NOHA, the situation is different. Although we found the water oxygen to be at least 0.5 Å further away from the NO ligand than in the X-ray structure, the ENDOR estimate for the nearby exchangeable proton position is in good agreement with the predicted position of the NH hydrogen atom of NOHA (black open circles in the bottom panel of

Figure 6). The nearby hydrogen atom forms an H-bond with the NO ligand, in agreement with the conclusions of the X-ray crystallographic work.^{4a}

To improve the agreement between the X-ray and ENDOR O_{water} positions, we have made an attempt to reconsider the spin density distribution in the Fe–N–O fragment of the heme center. As stated above, the ENDOR data were analyzed in terms of structure using $(\rho_{\text{Fe}}, \rho_{\text{N}}, \rho_{\text{O}}) = (0.2, 0.5, 0.3)$. The fact that the ENDOR distances estimated using these spin densities are significantly larger than those found in the crystal structures could be interpreted as implying that ρ_{N} and ρ_{O} are actually smaller than those we used. The analysis of all available data (both obtained here and in our earlier work¹¹) shows, however, that no satisfactory solution for this problem exists. For example, the spin density distribution required to match the ENDOR estimate of the water oxygen position in nNOS/Arg ($T_{\parallel} = -0.27$ MHz) with that obtained by X-ray is $(\rho_{\text{Fe}}, \rho_{\text{N}}, \rho_{\text{O}}) \approx (0.65, 0.22, 0.13)$ (assuming $\rho_{\text{O}}/\rho_{\text{N}} = 0.6$, as discussed above). Such a distribution, however, will place the guanidino nitrogen of the L-Arg substrate ($T_{\parallel} = 0.66$ MHz for ¹⁴N) at 1.8 Å from N(NO), which is approaching a covalent bonding distance (1.4–1.45 Å) and is therefore completely unrealistic. This distance is also significantly shorter than the X-ray crystallographic distance of about 3 Å. The H_ε proton of Phe 586 will be located at the estimated 1.65 Å from O(NO), also noticeably closer than the X-ray distance of 2.2 Å.

In the distribution discussed above, the overall spin density on the NO ligand was reduced in favor of the central Fe ion, but the ratio of $\rho_{\text{O}}/\rho_{\text{N}} = 0.6$ was retained. Alternatively, one can keep $\rho_{\text{N}} + \rho_{\text{O}} = 0.8$ constant but increase ρ_{N} at the expense of ρ_{O} . Because the water oxygen is closer to O(NO) than to N(NO) (on the basis of the crystal structures), this might also make the ENDOR estimates for ¹⁷O more similar to the X-ray distance. Dashed lines in Figures 4 and 6 show, as an example, the calculated possible positions for $(\rho_{\text{Fe}}, \rho_{\text{N}}, \rho_{\text{O}}) = (0.2, 0.7, 0.1)$, where most of the spin density is concentrated on the NO ligand nitrogen. Even such an extreme and totally unrealistic distribution, however, does not result in agreement between the ENDOR and X-ray oxygen positions. It also does not change our conclusions regarding the H-bonding situation because the closest possible positions the exchangeable proton in nNOS/NS and nNOS/Arg are on the border or barely within the formal H-bonding range (see the dashed lines in Figure 6).

We therefore confirm the conclusion of our previous work that the spin density distribution of $\sim (0.2, 0.5, 0.3)$ produces the most balanced results and is the most realistic one. Two kinds of reasons may be responsible for the deviations from the X-ray data. First, the changes could be attributed to the fact that the crystals for the X-ray investigation were grown from solutions at pH 5.6–6.0,^{4b} whereas our solution samples were prepared at pH 7.4. It is conceivable that the increase in pH could lead to minor nonspecific structural alterations. It could also result in the active site water molecule being replaced by a hydroxide, HO[−], which could dramatically change the hydrogen bonding situation at the heme active site. To test the potential effect of pH, we investigated a sample of nNOS/Arg at pH 6.0. The EPR and ENDOR spectra for this sample were identical to those of the sample prepared at pH 7.4 (Figure S8, Supporting Information). The effect of pH can thus be excluded from consideration.

Alternatively, the differences could be caused by structural restrictions imposed by the crystal packing, which are absent for the protein in solution. A certain degree of inherent structural

flexibility in the side chains could lead to subtle structural rearrangements (note that the absolute differences of the relevant distances are on the order of 1 Å) compared to the crystal structure. This implies, in particular, that in liquid solution the hydrogen bonding network at the heme active site is most likely dynamic, with the H-bonds forming, breaking, and switching between various partners in response to the relatively minor modifications of the local protein geometry. In some structural realizations (e.g., nNOS in a crystal^{4b}), the H-bond between the active site water and the NO ligand (or, the peroxy ligand in the case of ferric peroxy intermediate) required by the NOS mechanism is formed. In other structural realizations (like that observed in this work for nNOS/NS or nNOS/Arg in frozen solution), the NO ligand does not participate in the hydrogen bonding.

This dynamic model allows one to reconcile the absence of any H-bonding to the NO ligand in the nNOS/Arg sample (as observed in this work by pulsed ENDOR) with the proton availability (supposedly provided by the H-bonding) necessary for the cleavage of the O–O bond and subsequent hydroxylation of L-Arg to NOHA.^{4b,23} note that the NOS ferrous–NO complex is a close mimic of the obligatory ferric (hydro)peroxy intermediate in NOS catalysis.¹⁰ An attractive feature of this model is that it naturally allows the ligand, water, and substrate molecules to be readily incorporated into or released from the active site. An additional observation in support of this view is that in the eNOS–NO structure²⁴ the electron density for the water molecule near the NO ligand is weak even though the amino acids and the local protein structures surrounding the NO ligand are identical in eNOS²⁴ and nNOS.^{4b} Thus, the two crystal structures (nNOS and eNOS) represent the two extremes, ordered water and weakly bound water in the active site, whereas our present results provide a picture midway between these two extremes.

With this dynamic model, it is reasonable to expect that the specific H-bonding situation observed for a given NOS sample might depend on the NOS isoform, substrate, and the type of the heme complex. Indeed, the H-bonding situation for the nNOS/NOHA sample observed in this work is qualitatively similar to that in a crystal structure.^{4a} Another example is provided by the study of peroxyferri–NOS form in the cryo-reduced oxy–eNOS with Arg substrate, where a proton characterized by significant anisotropic and isotropic *hfi* (signifying the H-bond formation) was detected by ¹H ENDOR in the frozen solution sample, which was prepared at pH 7.4.^{7b}

It is also interesting to note that there is a correlation between the ENDOR structural results and the shape of the EPR spectra. The EPR spectra of nNOS/NS and nNOS/Arg are nearly identical, which correlates with the fact that in both preparations the NO ligand does not form hydrogen bonds with either water oxygen or the guanidino nitrogen of L-Arg substrate. In nNOS/NOHA, on the contrary, the NO ligand forms a hydrogen bond with the substrate (NOHA), which possibly results in a slight repositioning of this ligand and, as a consequence, in the change of the EPR spectrum (interestingly, the rhombic form of the EPR spectrum of myoglobin–NO, where the NO ligand participates in an H-bonding, has the principal *g*-values similar to those of nNOS/NOHA^{7c}). A minor redistribution of the electronic and spin density in the Fe–NO fragment caused by the H-bond could also contribute to the observed change of the EPR spectrum.

The nearby nonexchangeable hydrogen atom assigned as H_e of Phe584 was detected in all three samples. This hydrogen atom may have a stabilizing effect on the NO ligand and probably determines its position: H_e eclipses one of C_{meso} atoms of the heme, whereas the oxygen of NO eclipses a pyrrole nitrogen on either side of that C_{meso} (Figure S1, Supporting Information). On the basis of the NO– H_e distance of about 2.2 Å, it appears that there should be some specific interaction between the NO and H_e . Although the H-bond with a C–H hydrogen is traditionally believed impossible (because the CH bond is practically nonpolar), the existence of such bonds has been considered in the literature already for several decades, and lately such a concept was employed to explain protein structures.²⁵ One may speculate that such a specific interaction with H_e of Phe584 also exists in the native ferric– O_2 complex (the analog of which ferrous–NO represents), and it plays a role in positioning the peroxide ligand properly for the interaction with the substrate.

CONCLUSION

This investigation aimed to obtain direct information about the H-bonding network at the heme active site(s) of nNOS using the ferrous–NO mimic of the ferri–peroxo species. Unexpectedly, however, no H-bonding interactions connecting the NO ligand to the active site water molecule or Arg substrate were detected, in contrast to the results obtained earlier by X-ray crystallography for nNOSoxy containing the Arg substrate.^{4b} The nearby exchangeable proton in both the nNOS/NS and nNOS/Arg samples is located outside the H-bonding range and, on the basis of the obtained structural constraints, can belong to the active site water (or OH). On the contrary, in the NOHA-bound sample, the nearby exchangeable hydrogen forms an H-bond with the NO ligand (on the basis of its distance from the NO ligand and a nonzero isotropic hfi constant), but it does not belong to the active site water molecule because the water oxygen atom (detected by ^{17}O ENDOR) is too far. This hydrogen should therefore come from the NOHA substrate, which is in agreement with the X-ray work.^{4a}

The apparent contradiction between the lack of any H-bonding as observed for the NO ligand in nNOS/Arg by 1H pulsed ENDOR in this work and the necessity of such H-bonding for the hydroxylation of L-Arg to NOHA is rationalized by hypothesizing that in liquid solution the H-bonding network at the heme active site is most likely dynamic, with various transient H-bonds being formed in response to the relatively minor modifications of the local protein geometry. The specific H-bonding situations observed in the crystal (where the H-bond with the NO ligand is likely present) and in frozen solution (no H-bond with the NO ligand) correspond to somewhat different local structural realizations stabilized in these samples and are within the overall range of possible H-bonding situations realized in a liquid solution.

ASSOCIATED CONTENT

Supporting Information

Local structures of the heme active sites of nNOS/Arg showing orientational heterogeneity of the NO ligand; numerical first derivatives of the field sweep ESE spectra; numerical simulation of the ESE field sweep spectrum of the impurity signal at $g = 2.027$; orientation-selective 1H and ^{17}O ENDOR spectra; analysis of the ^{17}O ENDOR spectra; comparison between the nNOS/Arg 1H ENDOR spectra at pH 6.0 and 7.4; preparation

details of the nNOS/Arg sample at pH 6.0; Euler angles definition. The Supporting Information is available free of charge on the ACS Publications website at DOI: 10.1021/acs.jpca.5b01804.

AUTHOR INFORMATION

Corresponding Author

*Changjian Feng. Phone: 505-925-4326. Fax: 505-925-4549. E-mail: cfeng@unm.edu.

Notes

The authors declare no competing financial interest.

ACKNOWLEDGMENTS

This work was supported by NIH GM081811 to C.F., NSF CHE-1150644 to C.F., AHA Grant-in-Aid 12GRNT11780019 to C.F., NIH GM57353 to T.L.P., and NIH GM052419 to L.J.R. A.V.A. gratefully acknowledges the NSF (DBI-0139459, DBI-9604939, BIR-9224431) and NIH (S10RR020959, S10RR026416-01) grants for the development of the EPR facility at the University of Arizona.

REFERENCES

- (1) Alderton, W. K.; Cooper, C. E.; Knowles, R. G. Nitric Oxide Synthases: Structure, Function and Inhibition. *Biochem. J.* **2001**, *357*, 593–615.
- (2) (a) Woodward, J. J.; Chang, M. M.; Martin, N. I.; Marletta, M. A. The Second Step of the Nitric Oxide Synthase Reaction: Evidence for Ferric-Peroxo as the Active Oxidant. *J. Am. Chem. Soc.* **2009**, *131* (1), 297–305. (b) Zhu, Y.; Silverman, R. B. Revisiting Heme Mechanisms. A Perspective on the Mechanisms of Nitric Oxide Synthase (NOS), Heme Oxygenase (HO), and Cytochrome P450s (Cyp450s). *Biochemistry* **2008**, *47* (8), 2231–2243.
- (3) (a) Hannibal, L.; Page, R. C.; Haque, M. M.; Bolisetty, K.; Yu, Z.; Misra, S.; Stuehr, D. J. Dissecting Structural and Electronic Effects in Inducible Nitric Oxide Synthase. *Biochem. J.* **2015**, *467* (1), 153–65. (b) Crane, B. R.; Sudhamsu, J.; Patel, B. A. Bacterial Nitric Oxide Synthases. *Annu. Rev. Biochem.* **2010**, *79* (1), 445–470. (c) Santolini, J. The Molecular Mechanism of Mammalian NO-Synthases: A Story of Electrons and Protons. *J. Inorg. Biochem.* **2011**, *105* (2), 127–141.
- (4) (a) Doukov, T.; Li, H. Y.; Soltis, M.; Poulos, T. L. Single Crystal Structural and Absorption Spectral Characterizations of Nitric Oxide Synthase Complexed with N^{ω} -Hydroxy-L-Arginine and Diatomic Ligands. *Biochemistry* **2009**, *48* (43), 10246–10254. (b) Li, H. Y.; Igarashi, J.; Jamal, J.; Yang, W. P.; Poulos, T. L. Structural Studies of Constitutive Nitric Oxide Synthases with Diatomic Ligands Bound. *J. Biol. Inorg. Chem.* **2006**, *11* (6), 753–768.
- (5) Hoffman, B. M. Electron-Nuclear Double Resonance Spectroscopy (and Electron Spin-Echo Envelope Modulation Spectroscopy) in Bioinorganic Chemistry. *Proc. Natl. Acad. Sci. U. S. A.* **2003**, *100* (7), 3575–3578.
- (6) de Vera, I. M. S.; Blackburn, M. E.; Galiano, L.; Fanucci, G. E., Pulsed EPR Distance Measurements in Soluble Proteins by Site-Directed Spin Labeling (SDSL). *Current Protocols in Protein Science*; John Wiley & Sons, Inc.: New York, 2013.
- (7) (a) Astashkin, A. V.; Kawamori, A.; Kodera, Y.; Kuroiwa, S.; Akabori, K. An Electron Spin Echo Envelope Modulation Study of the Primary Acceptor Quinone in Zn-Substituted Plant Photosystem II. *J. Chem. Phys.* **1995**, *102* (14), 5583–5588. (b) Davydov, R.; Ledbetter-Rogers, A.; Martasek, P.; Larukhin, M.; Sono, M.; Dawson, J. H.; Masters, B. S. S.; Hoffman, B. M. EPR and ENDOR Characterization of Intermediates in the Cryoreduced Oxy-Nitric Oxide Synthase Heme Domain with Bound L-Arginine or N-G-Hydroxyarginine. *Biochemistry* **2002**, *41* (33), 10375–10381. (c) Radoul, M.; Sundararajan, M.; Potapov, A.; Riplinger, C.; Neese, F.; Goldfarb, D. Revisiting the Nitrosyl Complex of Myoglobin by High-Field Pulse EPR Spectroscopy and Quantum Mechanical Calculations. *Phys. Chem. Chem. Phys.* **2009**, *11*, 10375–10381.

- 691 **2010**, 12 (26), 7276–7289. (d) Radoul, M.; Bykov, D.; Rinaldo, S.;
692 Cutruzzolà, F.; Neese, F.; Goldfarb, D. Dynamic Hydrogen-Bonding
693 Network in the Distal Pocket of the Nitrosyl Complex of *Pseudomonas*
694 *Aeruginosa* cd_1 Nitrite Reductase. *J. Am. Chem. Soc.* **2011**, 133 (9),
695 3043–3055.
- 696 (8) Davydov, R.; Sudhamsu, J.; Lees, N. S.; Crane, B. R.; Hoffman, B.
697 M. EPR and ENDOR Characterization of the Reactive Intermediates
698 in the Generation of NO by Cryoreduced Oxy-Nitric Oxide Synthase
699 from *Geobacillus Stearothermophilus*. *J. Am. Chem. Soc.* **2009**, 131
700 (40), 14493–14507.
- 701 (9) Davydov, R.; Labby, K. J.; Chobot, S. E.; Lukoyanov, D. A.;
702 Crane, B. R.; Silverman, R. B.; Hoffman, B. M. Enzymatic and
703 Cryoreduction EPR Studies of the Hydroxylation of Methylated N^ω -
704 Hydroxy-L-Arginine Analogues by Nitric Oxide Synthase from
705 *Geobacillus Stearothermophilus*. *Biochemistry* **2014**, 53 (41), 6511–
706 6519.
- 707 (10) (a) Couture, M.; Adak, S.; Stuehr, D. J.; Rousseau, D. L.
708 Regulation of the Properties of the Heme-NO Complexes in Nitric-
709 Oxide Synthase by Hydrogen Bonding to the Proximal Cysteine. *J.*
710 *Biol. Chem.* **2001**, 276 (41), 38280–38288. (b) Migita, C. T.; Salerno,
711 J. C.; Masters, B. S. S.; Martasek, P.; McMillan, K.; IkedaSaito, M.
712 Substrate Binding-Induced Changes in the EPR Spectra of the Ferrous
713 Nitric Oxide Complexes of Neuronal Nitric Oxide Synthase.
714 *Biochemistry* **1997**, 36 (36), 10987–10992.
- 715 (11) Astashkin, A. V.; Elmore, B. O.; Chen, L.; Fan, W.; Guillemette,
716 J. G.; Feng, C. Pulsed ENDOR Determination of the Arginine
717 Location in the Ferrous–NO Form of Neuronal NOS. *J. Phys. Chem. A*
718 **2012**, 116 (25), 6731–6739.
- 719 (12) (a) Feng, C. J.; Tollin, G.; Hazzard, J. T.; Nahm, N. J.;
720 Guillemette, J. G.; Salerno, J. C.; Ghosh, D. K. Direct Measurement by
721 Laser Flash Photolysis of Intraprotein Electron Transfer in a Rat
722 Neuronal Nitric Oxide Synthase. *J. Am. Chem. Soc.* **2007**, 129 (17),
723 5621–5629. (b) Ghosh, D. K.; Holliday, M. A.; Thomas, C.;
724 Weinberg, J. B.; Smith, S. M. E.; Salerno, J. C. Nitric-Oxide Synthase
725 Output State - Design and Properties of Nitric-Oxide Synthase
726 Oxygenase/FMN Domain Constructs. *J. Biol. Chem.* **2006**, 281 (20),
727 14173–14183. (c) Ghosh, D. K.; Wu, C. Q.; Pitters, E.; Moloney, M.;
728 Werner, E. R.; Mayer, B.; Stuehr, D. J. Characterization of the
729 Inducible Nitric Oxide Synthase Oxygenase Domain Identifies a 49
730 Amino Acid Segment Required for Subunit Dimerization and
731 Tetrahydrobiopterin Interaction. *Biochemistry* **1997**, 36 (35), 10609–
732 10619.
- 733 (13) Glasoe, P. K.; Long, F. A. Use of Glass Electrodes to Measure
734 Acidities in Deuterium Oxide. *J. Phys. Chem.* **1960**, 64 (1), 188–190.
- 735 (14) Astashkin, A. V.; Enemark, J. H.; Raitsimring, A. 26.5–40 GHz
736 K_α -band Pulsed EPR Spectrometer. *Concepts Magn. Reson., Part B*
737 **2006**, 29B (3), 125–136.
- 738 (15) Mims, W. B. Pulsed ENDOR Experiments. *Proc. R. Soc. London,*
739 *Ser. A* **1965**, 283 (1395), 452–457.
- 740 (16) Doan, P. E.; Hoffman, B. M. Making Hyperfine Selection in
741 Mims ENDOR Independent of Deadtime. *Chem. Phys. Lett.* **1997**, 269
742 (3–4), 208–214.
- 743 (17) Astashkin, A. V. Simbud. [http://www.cbc.arizona.edu/facilities/](http://www.cbc.arizona.edu/facilities/epr_facility_software)
744 [epr_facility_software](http://www.cbc.arizona.edu/facilities/epr_facility_software).
- 745 (18) (a) Patchkovskii, S.; Ziegler, T. Structural Origin of Two
746 Paramagnetic Species in Six-Coordinated Nitrosoiron(II) Porphyrins
747 Revealed by Density Functional Theory Analysis of the G Tensors.
748 *Inorg. Chem.* **2000**, 39 (23), 5354–5364. (b) Praneeth, V. K. K.;
749 Neese, F.; Lehnert, N. Spin Density Distribution in Five- and Six-
750 Coordinate Iron(II)–Porphyrin NO Complexes Evidenced by
751 Magnetic Circular Dichroism Spectroscopy. *Inorg. Chem.* **2005**, 44
752 (8), 2570–2572. (c) Praneeth, V. K. K.; Haupt, E.; Lehnert, N.
753 Thiolate Coordination to Fe(II)-Porphyrin NO Centers. *J. Inorg.*
754 *Biochem.* **2005**, 99 (4), 940–948.
- 755 (19) Praneeth, V. K. K.; Näther, C.; Peters, G.; Lehnert, N.
756 Spectroscopic Properties and Electronic Structure of Five- and Six-
757 Coordinate Iron(II) Porphyrin NO Complexes: Effect of the Axial N-
758 Donor Ligand. *Inorg. Chem.* **2006**, 45 (7), 2795–2811.
- (20) Lehnert, N. The spin populations of N and O predicted by DFT 759
are about 0.5 and 0.3, respectively. Private communication. 760
- (21) (a) Astashkin, A. V.; Klein, E. L.; Enemark, J. H. Toward 761
Modeling the High Chloride, Low pH Form of Sulfite Oxidase: K_α - 762
band ESEEM of Equatorial Chloro Ligands in Oxomolybdenum(V) 763
Complexes. *J. Inorg. Biochem.* **2007**, 101 (11–12), 1623–1629. 764
(b) Astashkin, A. V.; Johnson-Winters, K.; Klein, E. L.; Byrne, R. S.; 765
Hille, R.; Raitsimring, A. M.; Enemark, J. H. Direct Demonstration of 766
the Presence of Coordinated Sulfate in the Reaction Pathway of 767
Arabidopsis Thaliana Sulfite Oxidase Using ^{33}S Labeling and ESEEM 768
Spectroscopy. *J. Am. Chem. Soc.* **2007**, 129 (47), 14800–14810. 769
- (22) (a) O’Keeffe, D. H.; Ebel, R. E.; Peterson, J. A. Studies of the 770
Oxygen Binding Site of Cytochrome P-450. Nitric Oxide as a Spin- 771
Label Probe. *J. Biol. Chem.* **1978**, 253 (10), 3509–3516. (b) Tsubaki, 772
M.; Hiwatashi, A.; Ichikawa, Y.; Hori, H. Electron Paramagnetic 773
Resonance Study of Ferrous Cytochrome P-450 sc -Nitric Oxide 774
Complexes: Effects of Cholesterol and Its Analogs. *Biochemistry* **1987**, 775
26 (14), 4527–4534. 776
- (23) Li, D.; Kabir, M.; Stuehr, D. J.; Rousseau, D. L.; Yeh, S. R. 777
Substrate- and Isoform-Specific Dioxxygen Complexes of Nitric Oxide 778
Synthase. *J. Am. Chem. Soc.* **2007**, 129 (21), 6943–6951. 779
- (24) Li, H. Y.; Raman, C. S.; Martasek, P.; Masters, B. S. S.; Poulos, 780
T. L. Crystallographic Studies on Endothelial Nitric Oxide Synthase 781
Complexed with Nitric Oxide and Mechanism-Based Inhibitors. 782
Biochemistry **2001**, 40 (18), 5399–5406. 783
- (25) (a) Brandl, M.; Lindauer, K.; Meyer, M.; Sühnel, J. C–H \cdots O 784
and C–H \cdots N Interactions in RNA Structures. *Theor. Chem. Acc.* **1999**, 785
101 (1–3), 103–113. (b) Sarkhel, S.; Desiraju, G. R. N–H \cdots O, O–H \cdots 786
O, and C–H \cdots O Hydrogen Bonds in Protein–Ligand Complexes: 787
Strong and Weak Interactions in Molecular Recognition. *Proteins:* 788
Struct., Funct., Genet. **2004**, 54 (2), 247–259. (c) Madan Babu, M.; 789
Kumar Singh, S.; Balaram, P. A C–H \cdots O Hydrogen Bond Stabilized 790
Polypeptide Chain Reversal Motif at the C Terminus of Helices in 791
Proteins. *J. Mol. Biol.* **2002**, 322 (4), 871–880. (d) Derewenda, Z. S.; 792
Lee, L.; Derewenda, U. The Occurrence of C–H \cdots O Hydrogen 793
Bonds in Proteins. *J. Mol. Biol.* **1995**, 252 (2), 248–262. (e) Bonchev, 794
D.; Cremaschi, P. C–H Group as Proton Donor by Formation of a 795
Weak Hydrogen Bond. *Theoret. Chim. Acta* **1974**, 35 (1), 69–80. 796